

# Soft Matter

Accepted Manuscript



This is an *Accepted Manuscript*, which has been through the Royal Society of Chemistry peer review process and has been accepted for publication.

*Accepted Manuscripts* are published online shortly after acceptance, before technical editing, formatting and proof reading. Using this free service, authors can make their results available to the community, in citable form, before we publish the edited article. We will replace this *Accepted Manuscript* with the edited and formatted *Advance Article* as soon as it is available.

You can find more information about *Accepted Manuscripts* in the [Information for Authors](#).

Please note that technical editing may introduce minor changes to the text and/or graphics, which may alter content. The journal's standard [Terms & Conditions](#) and the [Ethical guidelines](#) still apply. In no event shall the Royal Society of Chemistry be held responsible for any errors or omissions in this *Accepted Manuscript* or any consequences arising from the use of any information it contains.

Cite this: DOI: 10.1039/xxxxxxxxxx

## Coarse-grained molecular simulations of the melting kinetics of small unilamellar vesicles<sup>†</sup>

Lara A. Patel,<sup>\*a</sup> and James T. Kindt<sup>a</sup>Received Date  
Accepted Date

DOI: 10.1039/xxxxxxxxxx

www.rsc.org/journalname

Simulations of small unilamellar lipid bilayer vesicles have been performed to model their response to an instantaneous rise in temperature, starting from an initial low-temperature structure to temperatures near or above the main chain transition temperature. The MARTINI coarse-grained force-field was used to construct slabs of gel-phase DPPC bilayers, which were assembled into truncated icosahedral structures containing 13,165 or 31,021 lipids. Equilibration at 280 K produced structures with several (5-8) domains, characterized by facets of lipids packed in the gel phase connected by disordered ridges. Instantaneous heating to final temperatures ranging from 290 K to 310 K led to partial or total melting over 500 ns trajectories, accompanied by changes in vesicle shape and the sizes and arrangements of remaining gel-phase domains. At temperatures that produced partial melting, the gel-phase lipid content of the vesicles followed an exponential decay, similar in form and timescale to the sub-microsecond phase of melting kinetics observed in recent ultrafast IR temperature-jump experiments. The changing rate of melting appears to be the outcome of a number of competing contributions, but changes in curvature stress arising from the expansion of the bilayer area upon melting are a major factor. The simulations give a more detailed picture of the changes that occur in frozen vesicles following a temperature jump, which will be of use for the interpretation of temperature-jump experiments on vesicles.

### 1 Introduction

Unilamellar vesicles are closed bilayers encapsulating an internal volume of solvent. The bilayer consists of amphiphilic lipids that self-assemble to sequester hydrophobic tail groups from polar solvent. With vesicles spanning size scales from the nm to  $\mu\text{m}$ , there are three subcategories: small unilamellar vesicles (SUV) with diameters less than 100 nm, large unilamellar vesicles (LUV) 100 nm to 1  $\mu\text{m}$  in diameter, and giant unilamellar vesicles (GUV) with diameters exceeding 1  $\mu\text{m}$ .<sup>1</sup> Vesicles are convenient simple model systems for biomembranes, and can also be used as nanoencapsulation agents for drug delivery and related functions.

The phase behavior of lipids in vesicles has been the subject of a number of experimental and computational studies, and has been exploited in the use of liposomes as thermosensitive drug delivery agents,<sup>2,3</sup> that change their permeability at the phase transition temperature  $T_m$ .<sup>4</sup> Here our primary goal is to model the dynamics of phase change when a vesicle undergoes partial or total melting in response to a jump in temperature, a phenomenon observed in recent experiments by Nagarajan et al.<sup>5</sup> In that study, an ultrafast

IR laser pulse initiated a temperature jump in a solution of LUV's of deuterated dipalmitoyl phosphatidylcholine (DPPC) near the main chain transition temperature ( $T_m$ ), and the resulting change in phase was followed by time-resolved IR spectroscopy. A motivation for that study was to develop a method to induce a rapid change in the environment of lipid-associated proteins, so that the dynamics of their response can then be followed through time-dependent probe spectroscopies just as is common in T-jump experiments on soluble protein folding.<sup>6</sup> Understanding the evolving structure of the vesicle following a rapid temperature jump is important to fully interpret protein responses in future experiments.

The melting process studied by Nagarajan et al.<sup>5</sup> was fit to two distinct stages. A fast, single-exponential submicrosecond component of the transition was interpreted as an initial partial melting from preexisting defect sites. With atomistic molecular dynamics (MD) simulation data of melting bent lamellar sheets as supporting evidence, pre-melted ridges present at the contact between facets of rigid gel domains were proposed as the sites of these defects. Faceted structures have been observed in frozen vesicles imaged by electron microscopy<sup>7</sup> and simulated using coarse-grained<sup>8-11</sup> and lattice models<sup>12,13</sup>. In the second stage, melting slowed down and entered a stretched-exponential phase, which was attributed to complex coupled rearrangements of domains

<sup>a</sup> Emory University, Chemistry Department, 1515 Dickey Drive, Atlanta, GA 30322, USA. Fax: XX XXXX XXXX; Tel: +1 404 712 2983; E-mail: lapatel@emory.edu; E-mail: jkindt@emory.edu

<sup>†</sup> Electronic Supplementary Information (ESI) available: [details of any supplementary information available should be included here]. See DOI: 10.1039/b000000x/

and the influx of water.

The goal of this research is to gain a qualitative description of the melting phase transition of a vesicle and to establish if the kinetics qualitatively match experiment. To that end, we analyze the melting dynamics of simulated frozen vesicles of 13,165 and 31,021 DPPC lipids with diameters of 33 nm and 50 nm. We have found timescales for melting of single vesicles that are in good qualitative agreement with the bulk experimental values. In the current simulations we attempt to address the processes that take place during the sub-microsecond stage and the origin of the slowing-down in melting; the timescale for the second stage remains out of reach of our simulations, so we can only offer speculations.

The MARTINI 2.0 coarse-grained potential<sup>14,15</sup> was used for DPPC and for the accompanying coarse-grained water. There are some discrepancies between the phase behavior of this coarse-grained DPPC and the experimental DPPC. The experimental main phase transition temperature of DPPC is 314 K<sup>16</sup> (or 310 K for perdeuterated DPPC<sup>17–19</sup>), while estimates for the MARTINI model's transition temperature are lower, at  $295 \pm 5$  K<sup>14</sup> or  $302 \pm 1$  K<sup>20</sup>. A more important, qualitative difference is that the simulation model exhibits a direct transition from an untilted gel phase ( $L_\beta$ ) to the fluid phase ( $L_\alpha$ ), while true DPPC undergoes a pretransition from a tilted gel phase ( $L_{\beta'}$ ) to the ripple phase ( $P_{\beta'}$ ) and then to the fluid phase at  $T_m$ . The absence of tail tilt and the ripple phase in the simulation model simplifies the behavior of the phase transition.

The MARTINI version of DPPC has in common with the experimental system that it undergoes a considerable increase in area per lipid upon melting, from 0.48 nm<sup>2</sup> to 0.63 nm<sup>2</sup> in experiment<sup>21–26</sup> and from 0.47 to 0.64 nm<sup>2</sup> in the simulation model<sup>14</sup>. Over the initial microseconds of melting following the temperature jump, the area of the vesicle will expand. Given that the water content of LUV's responds to perturbations on a timescale of 10's of milliseconds<sup>27</sup> the solvent content and internal volume remains effectively constant over the initial stages of melting, meaning that melting will induce changes in local curvature and overall vesicle shape. Nagarajan et al.<sup>5</sup> rationalized the initial single-exponential melting dynamics by assuming that surface pressure builds up linearly with the degree of melting. In this study, the availability of actual structures will afford a more nuanced view of how the shape changes produced by melting feed back into the melting rate through surface curvature and interfacial line tension effects.

## 2 Methods

Molecular dynamics simulations are performed using GRO-MACS 4.6<sup>28–31</sup> and the MARTINI 2.0 coarse-grained (CG) force field<sup>14,15</sup> for DPPC lipids, water and anti-freeze (included as 10% of all solvent particles for vesicle simulations). CG anti-freeze particles effectively lower the water freezing temperature from  $\sim 290$  K to below 250 K.<sup>15</sup>

A time increment of 25 fs is used for all simulations. Temperature and pressure are kept constant using velocity-rescaling temperature coupling<sup>32</sup> with a time constant of  $\tau_T = 1.0$  ps and Berendsen pressure coupling<sup>33</sup> with a time constant  $\tau_p = 2.5$  ps

and a compressibility of  $\kappa = 5 \times 10^{-5}$  bar<sup>-1</sup>. Pressure coupling is fully isotropic for vesicle simulations and semi-isotropic (allowing the bilayer area to equilibrate independently of the normal dimension) for patch simulations. Graphical images of molecules were prepared using VMD.<sup>34</sup>

### 2.1 Bilayer patch simulations

A bilayer patch of 512 MARTINI DPPC lipids and 3656 CG water particles are equilibrated at 273 K and 1 bar for 600 ns. A similar simulation at 323 K and 1 bar is equilibrated for 200 ns to provide a base line for the fluid phase lipids. The average surface area per lipid is 0.46 nm<sup>2</sup> for the gel phase in agreement with simulation<sup>14</sup> and experimental values<sup>24–26</sup> and 0.64 nm<sup>2</sup> for the fluid phase, also in agreement with simulation<sup>14</sup> and experiment<sup>21–23,26</sup>.

### 2.2 Vesicle construction and solvation

Previous simulation studies of forming a gel-phase vesicle by freezing encountered delays associated with the release of internal solvent through pores and with pore closure.<sup>8</sup> Direct construction of a gel-phase vesicle via assembly of bilayer slabs into a truncated icosahedron was used here instead.

The advantage of a truncated icosahedron starting structure for vesicle simulations is the speed with which a stable vesicle structure in the gel phase is achieved. Truncated icosahedrons consist of 12 pentagonal faces and 20 hexagonal faces and closely approximate a spherical shape, while encouraging faceting similar to that observed in other vesicle freezing simulations.<sup>8,9</sup> Starting structures were prepared in three ways: with the pentagonal faces excluded to create 12 pores that serve as defect sinks, with all of the faces present and displaced from the origin sufficiently to prevent any bad contacts between lipids, and lastly with the faces displaced closer to the origin so that the bilayers overlap initially. If a pair of lipids are within 0.45 nm of each other, one of the lipids is removed. The first two methods lead to pores that take a long time to close (in excess of 1  $\mu$ s). The last structure leads to a stable and closed structure within 1  $\mu$ s that is used as a starting structure for all subsequent temperature-jump simulations.

To prepare this structure, larger gel phase bilayer slabs are constructed by removing solvent from the final bilayer patch structure at 273 K and replicating the membrane in the xy-plane. The large slab is cut into pentagonal and hexagonal slabs by lipid removal. Assembly of these pentagonal and hexagonal slabs into a truncated icosahedron is detailed in the supplementary information.

Vesicles are solvated with CG solvent containing 10% antifreeze at an initial density of 895 kg/m<sup>3</sup>, obtained by equilibration at 1 bar pressure and 300 K. Solvent particles within 0.6 nm of lipid beads are removed.

A summary of the final truncated icosahedron structure constants is given in Table 1.

### 2.3 Vesicle equilibration

The smaller vesicle (13,165 lipids) truncated icosahedron starting structure is run for 100 ns at 260 K and a pressure of 1 bar to

**Table 1** Summary of the total number of lipids in the initial truncated icosahedrons before removing bad contact lipids ( $N_{\text{Lipids},i}$ ), the final number of lipids after lipids with bad contacts are removed from the structure ( $N_{\text{Lipids},f}$ ), the radial displacement of the pentagon and hexagon slabs ( $r_{\text{slab}}$ ), the edge length of the slabs ( $l_{\text{edge}}$ ), the number of water particles ( $N_W$ ), and the number of anti-freeze particles ( $N_{\text{AF}}$ ).

$N_{\text{Lipids},i}$	$N_{\text{Lipids},f}$	$r_{\text{slab}}/\text{nm}$	$l_{\text{edge}}/\text{nm}$	$N_W$	$N_{\text{AF}}$
19,060	13,165	16.637	8.00	979,144	111,053
39,876	31,021	24.957	11.50	3,062,267	347,324

ensure that the vesicle does not melt completely. The vesicle is then run for 1.1  $\mu\text{s}$  at 280 K, below the reported main phase transition temperature of  $295 \pm 5 \text{ K}^{15}$ . The transition from the gel phase to fluid phase tapers off after the first few nanoseconds as is shown in Section 3 but the merging of gel domains persists even after having reached a stable fraction of lipids in the gel phase.

The larger vesicle (31,021 lipids) truncated icosahedron structure is run for 1  $\mu\text{s}$  at 280 K and 1 bar.

#### 2.4 Temperature jump simulations

The equilibrated vesicle structure is subjected to temperature jumps with simulations for the smaller vesicle at 290 K, 295 K, 300 K, and 310 K and for the larger vesicle at 290 K, 295 K, 297 K, and 300K. These temperatures are situated around the lamellar phase transition temperature of  $295 \pm 5 \text{ K}$  to allow for simulations that undergo partial melting. These simulations are run for 500 ns at a pressure of 1 bar.

The configuration from the end of the 500 ns trajectory of the small vesicle simulated at 295 K is subjected to a refreezing simulation at 280 K and run for 1  $\mu\text{s}$  at a pressure of 1 bar.

Simulations for the smaller vesicle were performed on the XSEDE computational resource Trestles. Using five 32 processor nodes, the simulation completed 160 ns/day. Simulations of the larger vesicle were performed on Comet with five 24 processor nodes and completed 60 ns/day.

#### 2.5 Order parameter

During analysis of simulation results, each lipid is classified as being in the fluid or gel phase based on an order parameter. The curved surface of a vesicle necessitates an order parameter defined independently of the lipid plane.

An initial categorization of each lipid as having a gel-like or fluid-like configuration is made by calculating the angle  $\theta_T$  between its two tails. This angle is defined as the angle between vectors from C1 to C4 sites in each tail, as illustrated in Fig. 1.

$$\bar{v}_{T1} = \bar{v}_{C4A} - \bar{v}_{C1A} \quad (1)$$

$$\bar{v}_{T2} = \bar{v}_{C4B} - \bar{v}_{C1B} \quad (2)$$

$$\theta_T = \sin^{-1} \left( \frac{\|\bar{v}_{T1} \times \bar{v}_{T2}\|}{\|\bar{v}_{T1}\| \cdot \|\bar{v}_{T2}\|} \right) \quad (3)$$

Due to tight tail-tail packing in the ordered gel phase we anticipate that the two tails on a single gel phase lipid samples a limited range of conformations within a relatively small range of

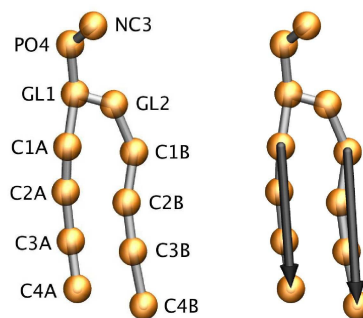


**Fig. 1** A single MARTINI 2.0 DPPC lipid with each coarse grain bead labeled and the tail vectors highlighted (black arrows).

angles  $\theta_T$ . The cutoff angle  $\theta_{\text{cut}}$  is  $15^\circ$  for gel phase lipids and was chosen based on the angle distribution of gel phase bilayer patch at 273 K (Fig. 2, blue curve) where a strong peak exists between  $0^\circ$  and  $20^\circ$ . By comparison the angle distribution of a fluid phase bilayer patch at 323 K is significantly broader (Fig. 2, orange curve).

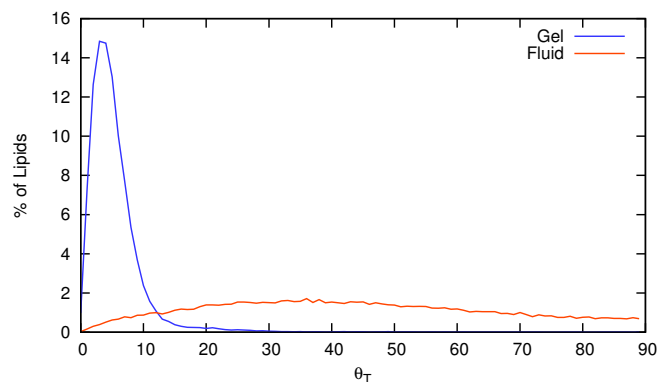


**Fig. 2** A plot of tail angle histogram for the bilayer patch of 512 DPPC lipids at 273 K (gel) and 323 K (fluid) averaged over the last 100 trajectory frames.

This choice of order parameter does not however account for local environment. Fluid phase lipids, while sampling a wider range of conformations and thus tail angles, still sample conformations with  $\theta_T \leq \theta_{\text{cut}}$ , as evident in the overlap of the two distributions in Fig. 2. Using only the internal order parameter to differentiate between the gel and fluid phase leads to an overestimation of the number of gel phase lipids. Lipids are therefore re-classified as fluid or gel according to their local environment: if 3 or more of a lipid's 6 nearest neighbors have  $\theta_T < 15^\circ$ , it is classified as belonging to the gel phase. The implementation of this classification is demonstrated in Fig. 3. Interfacial lipids are then defined as gel phase lipids that have one or more fluid phase neighbors.

#### 2.6 Relative shape anisotropy

The change in vesicle symmetry is quantitatively measured by the relative shape anisotropy,  $\kappa$ . The eigenvalues of the gyration ten-

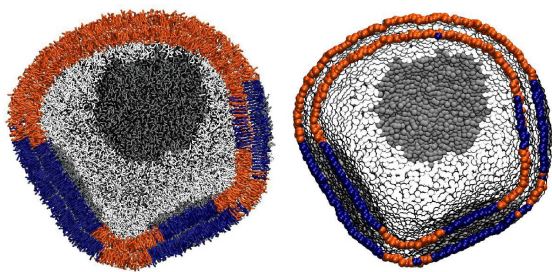


**Fig. 3** A snapshot of two cross sections of the same 13,165 lipid vesicle after melting at 290K, the left showing the full lipid structure and the right with a single bead per lipid. Each lipid is colored according to the local environment order parameter, orange being the fluid phase and blue the gel phase. Solvent although present in the simulations, is not shown in snapshots for clarity.

sor,

$$S_{m,n} = \frac{1}{N} \sum r_m r_n \quad (4)$$

$$\mathbf{S} = \begin{bmatrix} S_{xx} & S_{xy} & S_{xz} \\ S_{yx} & S_{yy} & S_{yz} \\ S_{zx} & S_{zy} & S_{zz} \end{bmatrix}, \quad (5)$$

are ordered such that  $S_1 \geq S_2 \geq S_3$  and  $\kappa$  is a function of those eigenvalues.<sup>35,36</sup>

$$\kappa = 1 - 3 \frac{S_1 S_2 + S_1 S_3 + S_2 S_3}{(S_1 + S_2 + S_3)^2} \quad (6)$$

When  $\kappa = 0$  the vesicle is spherically symmetric and  $\kappa = 1$  if the vesicle forms a line.

### 3 Results and Discussion

#### 3.1 Vesicle equilibration

Starting from the truncated icosahedron configurations, melting occurs at the vertices and edges of domains for both SUVs within the first couple of nanoseconds. The construction of the vesicle results in there being more free volume at the edges and vertices of the vesicle for melting to begin. The percentage of gel phase can be seen dropping from 100% to 60% followed by a recovery in the gel phase (Fig. 4). The vesicles reach a steady state with 59.4% of the lipids in the gel phase for the 13,165 lipid vesicle and 69.8% for the 31,021 lipid vesicle. The average diameters of the SUVs are 33.47 nm and 50.28 nm.

Although the truncated icosahedron starts with 32 distinct gel domains, both of the SUVs undergo a significant consolidation of those smaller domains. This is evident in the snapshots of the vesicles in Fig. 5 and 6. Consolidation of smaller domains results in a decrease in interfacial energy between the gel and fluid phase by decreasing the length of the interfaces.

In Fig. 7 the fraction of interfacial lipids with respect to the gel phase lipids is plotted, demonstrating that despite the majority of the melting and refreezing occurring within the first 200 ns of simulation, the decrease in interface takes longer.

Decreasing the interfacial fraction is observed to happen either by domain merging and/or by some domains melting away while

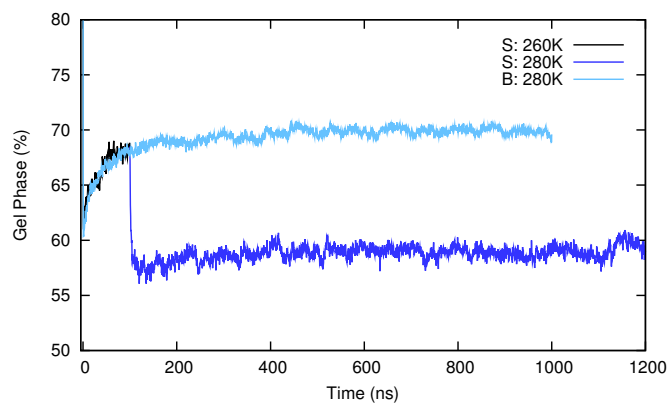


**Fig. 4** The percentage of gel phase lipids in the vesicle as it is equilibrated at 260 K (black) and then 280 K (blue) for the 13,165 lipid vesicle and 280K (light blue) for the 31,021 lipid vesicle.

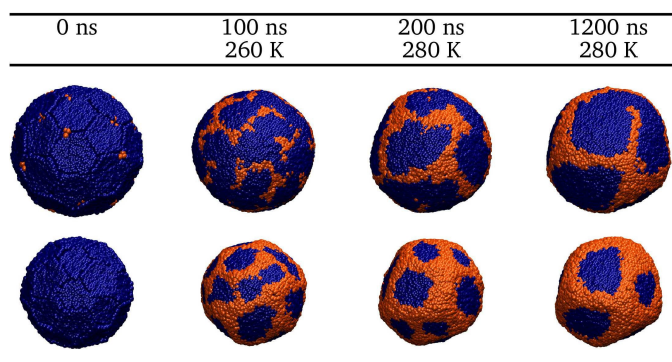


**Fig. 5** The 13165 lipid vesicle ( $d = 33$ nm) equilibration with the outer leaflet displayed in the upper row and the inner leaflet below with the gel (blue) and fluid (orange) phases shown. In the 1.2  $\mu$ s trajectory, the temperature is increased from 260 K to 280 K 100 ns into the trajectory once it is ascertained that the vesicle does not melt completely.

others growing as seen in Ostwald ripening (Section 3.5). Merging to decrease interfacial energy is coupled to an increase in the local curvature because fewer facets dictates sharper angles between facets. As discussed previously,<sup>12,13</sup> this curvature is localized along the fluid phase regions because the fluid phase has the lower bending modulus. Faceting is more pronounced in the smaller vesicle but present in both.

There is no lipid flip-flopping observed in any of the simulations, equilibration or otherwise. The smaller SUV has 41.8% of the lipids in the inner leaflet while the larger SUV has 44.7%. A disparity between the population of the inner and outer leaflets is expected due to the radii of the vesicles being so close in magnitude to the lamellar thickness<sup>14</sup> ( $4.0 \pm 0.1$  nm).

The phase composition is also asymmetric across the bilayer. In the smaller SUV 44.9% of the inner leaflet is in the gel phase as opposed to 69.8% in the outer leaflet. The larger vesicle exhibits 62.6% and 75.6% gel phase in the inner and outer leaflets respectively.

This disparity could be promoted by curvature environments in the inner and outer leaflets differing in magnitude and direction. The inner leaflet lipid tails are permitted a larger volume and thus are more prone to melting. The radii of the vesicles are on a simi-

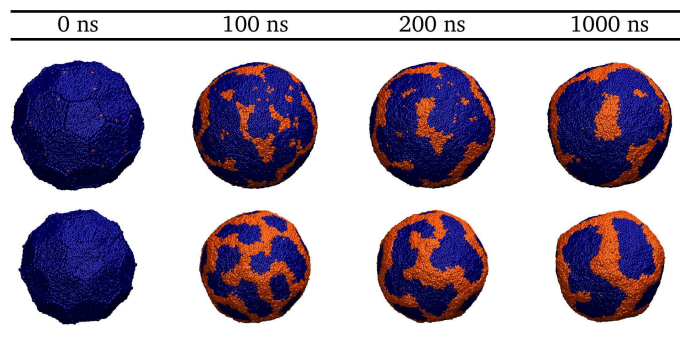


**Fig. 6** The 31,021 lipid vesicle ( $d = 50\text{nm}$ ) equilibration at 280 K with the outer leaflet displayed in the upper row and the inner leaflet below with the gel (blue) and fluid (orange) phases shown.

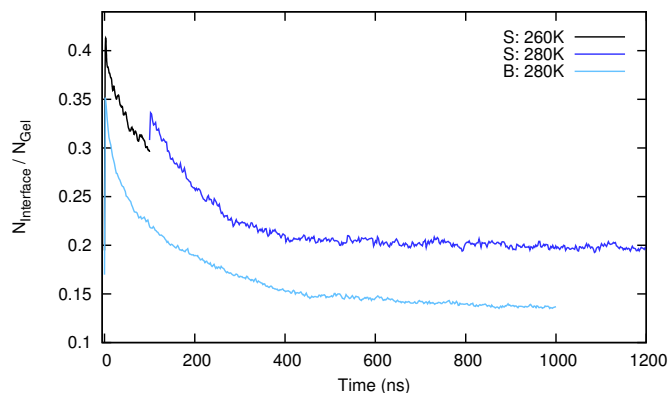


**Fig. 7** The fraction of interfacial lipids to gel phase lipids over the course of the equilibration runs.

lar magnitude to the thickness of the bilayer and as such the radii of curvature could be different enough to have an impact on the degree of melting. The difference in phase compositions could also be an artifact, introduced by the initial construction conditions, that under populates the inner leaflet and thus promotes conversion into the higher surface area phase to compensate. The phase transition being faster than lipid flip flopping, this would be a way of relaxing any inherent surface tension or pressure within each leaflet.<sup>37</sup>

### 3.2 Vesicle melting rates: Comparison with experiment

Partial melting is observed in the temperature-jump simulations for the small SUV (33 nm) at 290 K and 295 K and for the larger SUV (50 nm) at 290 K, 295 K, and 297 K. Averages over the final 100 ns of the temperature jump simulations are given in Table 2. Plots of the percentage of lipids in the gel phase for both vesicle sizes are shown in Fig. 8 with single exponential fits in black. The fit constants to the single exponential form:

$$f(t) = A \exp(-t/\tau) + C \quad (7)$$

are given in Table 3. On the 100 ns timescale they exhibit approximately single exponential melting kinetics in qualitative agreement with the early stages of melting measured in IR temperature-jump experiments.<sup>5</sup>

**Table 2** Averages and standard deviations over the last 100 ns (200 data points) of the melting simulations for the total, inner, and outer percentages of gel lipids ( $x_{\text{Gel}}$ ,  $x_{\text{Gel,i}}$ ,  $x_{\text{Gel,o}}$ ), the percentage of lipids in the inner leaflet ( $x_{\text{Inner}}$ ), and the number of gel domains for the inner ( $N_i$ ) and outer ( $N_o$ ) leaflets. The percentages of lipids in the inner leaflet are 41.8% and 44.7% respectively for the smaller and larger vesicle.

13,165 Lipids (33 nm)					
T/K	$x_{\text{Gel}}/\%$	$x_{\text{Gel,i}}/\%$	$x_{\text{Gel,o}}/\%$	$N_i$	$N_o$
280	$59.4 \pm 0.8$	$44.9 \pm 0.9$	$69.8 \pm 0.8$	6	8
290	$46.2 \pm 0.5$	$31.5 \pm 0.7$	$56.7 \pm 0.8$	5	5
295	$30.5 \pm 0.5$	$17.3 \pm 0.5$	$40.0 \pm 0.6$	2	3
300	$0.7 \pm 0.1$	$0.2 \pm 0.1$	$1.2 \pm 0.2$	0	0
310	$0.5 \pm 0.1$	$0.1 \pm 0.1$	$0.7 \pm 0.1$	0	0
280	$54.3 \pm 0.4$	$38.7 \pm 0.6$	$65.4 \pm 0.5$	2	3

31,021 Lipids (50 nm)					
T/K	$x_{\text{Gel}}/\%$	$x_{\text{Gel,i}}/\%$	$x_{\text{Gel,o}}/\%$	$N_i$	$N_o$
280	$69.8 \pm 0.3$	$62.6 \pm 0.5$	$75.6 \pm 0.4$	8	5
290	$61.3 \pm 0.3$	$52.8 \pm 0.5$	$68.2 \pm 0.4$	8	5
295	$51.7 \pm 0.3$	$44.0 \pm 3.1$	$57.7 \pm 0.6$	8	7
297	$41.4 \pm 0.5$	$35.0 \pm 0.4$	$46.5 \pm 0.6$	5	5
300	$0.7 \pm 0.1$	$0.3 \pm 0.1$	$1.1 \pm 0.2$	0	0

**Table 3** Fitting constants for the single exponential kinetics (Equations 7) exhibited by partially melted vesicles including the time constant  $\tau$  in simulation time units. Scale by 4 to compare to experimental time constants.

$N_{\text{Lipids}}$	T/K	$\tau/\text{ns}$	A	C
13,165	290	91.82	7.65	46.66
	295	131.28	20.81	29.84
31,021	290	85.35	3.15	61.65
	295	133.22	9.91	51.48
	297	165.96	18.69	40.72

The time constants ( $\tau$ ) are not expected to match experimental times exactly due to the effect of coarse-graining on the dynamics. Multiplying times from MARTINI model simulations by a factor of 4 to approximate experimental times has been suggested;<sup>14</sup> with this scaling factor, the range of timescales for melting in simulation (340 - 664 ns) matches that in experiment<sup>5</sup> (244 - 310 ns) to within a factor of 1.3 - 2.1.

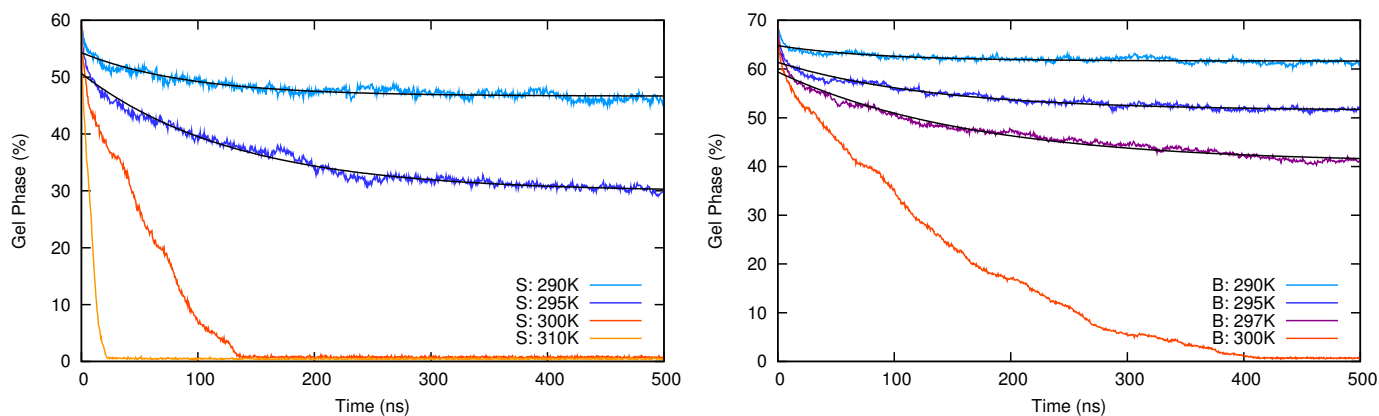
The experiments, in measuring changes in the gel-phase content averaged over an ensemble of vesicles, do not distinguish between gradual melting occurring over all the vesicles and rapid melting events distributed over a range of delay times. The qualitative similarity of the experimental ensemble average to simulated melting dynamics trends for individual vesicles strongly supports the former interpretation of the experimental data.

The initial fast melting ( $< 20\text{ns}$ ) does not fit well to the single exponential functional form indicating a different melting mechanism upon initial heating. A lack of sufficient time resolution may explain why this initial phase was not seen in experiment.

Experiments using T-jumps to final temperatures where the equilibrium state is fully melted did not yield a signal in ref. 5, presumably because the recovery time between laser shots was too short to permit nucleation of new gel-phase domains.

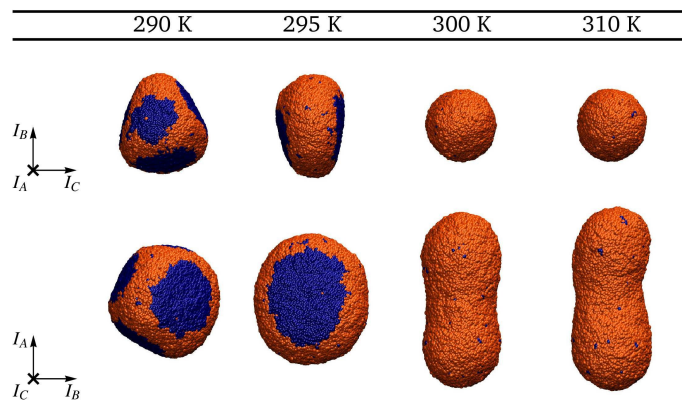
### 3.3 Vesicle melting: Structural changes

All of the vesicles exhibit some degree of shape change upon melting, evinced by the final structures of the 33 nm vesicle in Fig. 9



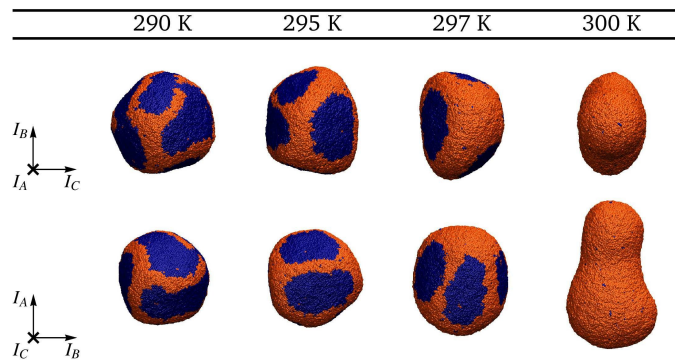
**Fig. 8** Percentage of gel phase lipids for a 33 nm SUV (left) melted at 290 K (cobalt blue), 295 K (blue), 300 K (orange), and 310 K (yellow) at 1 bar of pressure for 500 ns. Percentage of gel phase lipids for a 50 nm SUV (right) melted at 290 K (cobalt blue), 295 K (blue), 297 K (magenta), and 300 K (orange). Single exponential fits to the partially melted vesicles are shown in black.

or the 50 nm vesicle in Fig. 10. The number of domains (Table 2) in the case of the vesicle that remain relatively spherically symmetric are either static (the 50 nm vesicle at 290 K) or change only slightly (the 33 nm vesicle at 290 K and the 50 nm vesicle at 295 K).



**Fig. 9** Images of the 33 nm SUV after 500 ns temperature-jump simulations from 280 K to 290 K, 295 K, 297 K, and 300 K. The gel phase (blue) and fluid phase (orange) are shown. The two rows show the same vesicles viewed down the  $I_A$  (top) and the  $I_C$  (bottom) principle moment of inertia axes. Snapshots of these vesicles melting progression can be seen in Fig. S4 (see supplement).

The more drastic shape changes are coupled to a significant decrease in the number of domains. The partially melted 33 nm SUV at 295 K has asymmetric symmetry that appears to be converging on an oblate 'disk' shape, marred by a single gel domain in the outer leaflet with no matching inner domain. This domain would likely melt given a longer simulation. The approximately discoidal structure with two flat gel domains on opposite faces connected by a curved fluid-phase rim is appealingly symmetric and may represent a free energy minimum, or at least a long-lived intermediate state, for a partially melted small vesicle. A similar structure, with a single pair of gel domains present on opposite sides of a flattened (but less round) structure appears transiently during the complete melting of the 50 nm vesicle at 300 K. (See



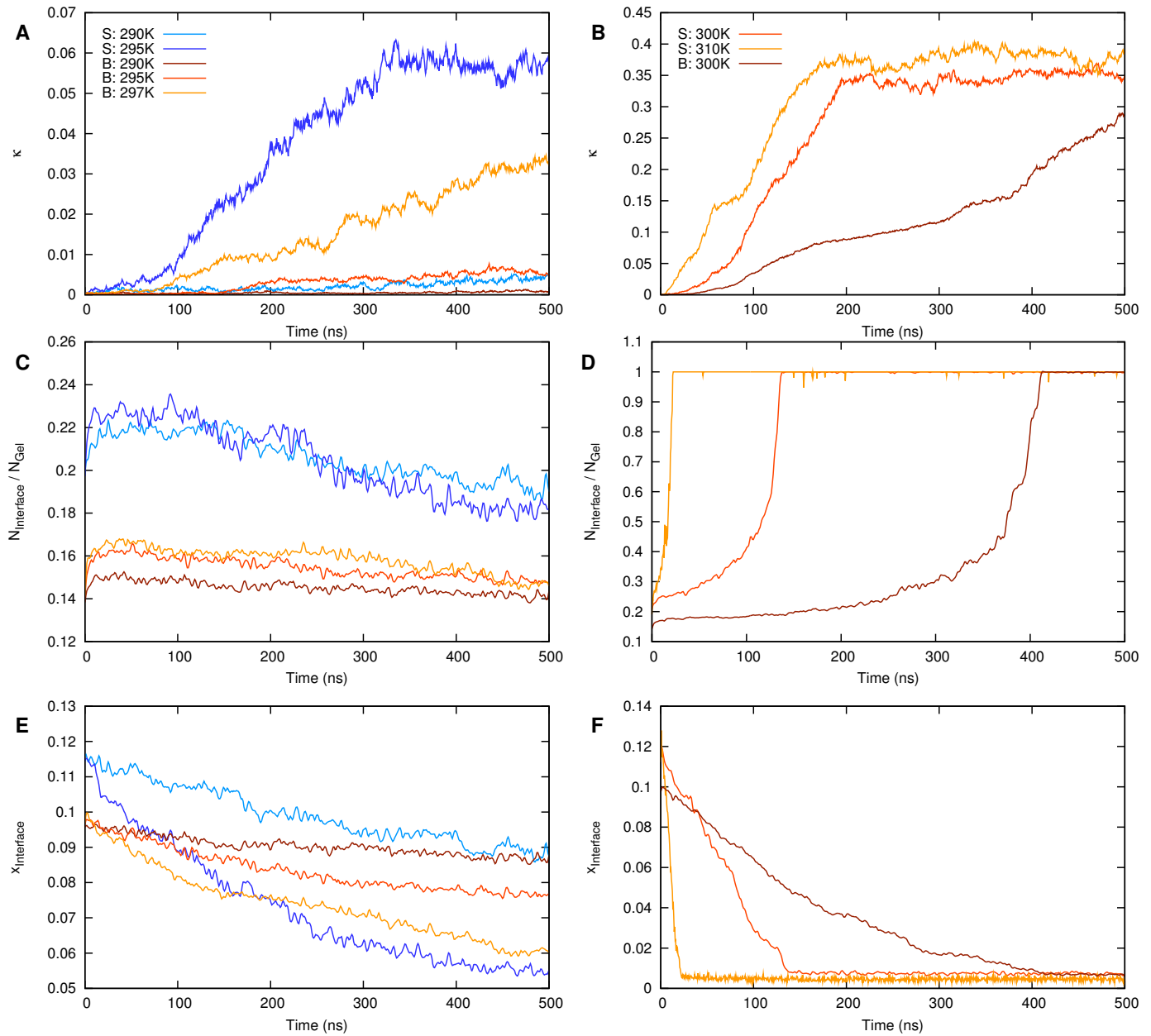
**Fig. 10** Images of the 50 nm SUV after 500 ns temperature-jump simulations from 280 K to 290 K, 295 K, 300 K, and 310 K. The gel phase (blue) and fluid phase (orange) are shown. The two rows show the same vesicles viewed down the  $I_A$  (top) and the  $I_C$  (bottom) principle moment of inertia axes. Snapshots of these vesicles melting progression can be seen in Fig. S5 (see supplement).

Fig. S6, supplemental information.) The 50 nm SUV at 297 K appears to be asymmetric as well.

Fig. 11 A and B plot the relative shape anisotropy ( $\kappa$ ), measuring the vesicles' symmetry as they undergo partial and full melting respectively. The small SUV at 295 K undergoes the most drastic shape change of the partially melted vesicles and appears to reach a steady state. The large vesicle at 297 K also shows a large shape change but it is clear from the plot that it has not reached a steady state.

Fig. 8 and Fig. 11 A show that changes in shape and the percentage of gel phase lipids occur simultaneously for the partially melted vesicles. After an initial ( $\sim 20$  ns) increase, the ratio of interfacial lipids to gel phase lipids steadily decreases throughout the trajectories (Fig. 11 C). Shape changes are accompanied by the melting and merging of domains, thereby decreasing the length of gel/fluid interfaces (Fig. 11 E). These shape changes include changes in curvature and thus curvature energy in the simulations.

Full melting is observed in the smaller SUV (33 nm) at 300 K and 310 K (Fig. 9) and for the larger SUV (50 nm) at 300 K (Fig.



**Fig. 11** Plot of the relative shape anisotropy  $\kappa$  for the partially melted vesicles (A) and the fully melted vesicles (B). (More detailed moment of inertial plots can be seen in Fig. S8.) Plot of the fraction of gel phase lipids at a gel-fluid interface for the partially melted vesicles (C) and the fully melted vesicles (D). Plot of the absolute fraction of lipids at the gel-fluid interfaces for the partially melted vesicles (E) and fully melted vesicles (F).

10) and produces structures with approximately prolate symmetry. Prolate or pear-shaped structures similar to those seen for the 33 nm vesicle and 50 nm vesicle respectively, have been reported as the elastically stable structures for moderately deflated vesicles;<sup>38</sup> a more quantitative comparison to those predictions is given in the next section.

### 3.4 Vesicle melting rates: Interpretation

To understand the connection between the changing rate of melting and the evolving vesicle structure we consider the mesoscale contributions to the structure's free energy.

The interplay between curvature energy, line tension, and domain shape in vesicles containing both ordered and fluid domains has been investigated through experiment<sup>39</sup> and theory<sup>40</sup> in the case of GUV's where long ribbon-like domains predominate.

Sknepnek et al.<sup>12</sup> have described faceted vesicle structures arising from the presence of a mixture of soft and stiff bending components with some interfacial free energy penalty governing their phase separation. The bending stress of the system is supported entirely by the soft component. The structures of partially melted vesicles seen here can be understood in the same framework, except that the fraction of the different mixing components is not fixed but determined by the equilibrium between gel and fluid phases.

The degree of melting in the vesicle is determined at equilibrium by minimization of a total free energy,

$$F_{tot} = F_0 + F_{interf} + F_{curv} \quad (8)$$

composed of the bending energy of the bilayer ( $F_{curv}$ ) and the interface between fluid and gel phases ( $F_{interf}$ ) in addition to the intrinsic free energy balance ( $F_0$ ) between gel and fluid phases. The state of the equilibrated vesicle before the temperature jump can be assumed to have reached a local minimum in this overall free energy with respect to the degree of melting at the edge of each gel domain:

$$\frac{dF}{d\Delta N} = 0 \quad (9)$$

where  $\Delta N = N_f - N_g$  is the difference between the number of fluid and gel phase lipids. Throughout this discussion, we will assume the constraints of constant total number of lipids, constant internal volume and constant number of lipids in each leaflet, the latter two imposed by the slow rates of permeability and flip-flop.

For a system brought out of equilibrium through a temperature jump, it is reasonable to assume that melting rate is determined both by the length of the gel/fluid interface and the magnitude of this driving force. The total interfacial length does not change enough (Fig. 11 E) to account for the near total slowing down observed (Fig. 8), so we look to each free energy component to identify how its derivative with respect to phase composition will evolve during melting. The first, intrinsic or bulk term in the full free energy can be approximated as:

$$F_0 \approx N_f \Delta H \left(1 - \frac{T}{T_m}\right) \quad (10)$$

using the fully frozen, planar bilayer as a reference. The deriva-

**Table 4** Critical nucleus sizes ( $N^*$ ) for a leaflet of a bilayer based on Equation 12 for temperatures below the bulk phase transition temperature (302 K) and a corresponding estimate of the diameter ( $d^*$ ) of a circular domain consisting of that many lipids. For the MARTINI DPPC model with a bilayer line tension  $\Lambda$  of  $10.0 \pm 1.5$  pN,<sup>20,42</sup> a conversion enthalpy  $\Delta H$  of  $25.8 \pm 1.5$  kJ/mol per molecule,<sup>20</sup> and a bulk phase transition temperature  $T_m$  of 302 K<sup>20</sup>. The approximate diameter ranges for domains in the inner ( $d_i$ ) and outer ( $d_o$ ) leaflets of the two vesicle sizes are reported based on structures at the end of the trajectories.

T/K	280	290	295	297	300
$N^*$	4	12	37	72	449
$d^*/\text{nm}$	1.5	2.7	4.6	6.4	16.2
33 nm Vesicle					
$d_i/\text{nm}$	9-16	6-20	12-18	-	-
$d_o/\text{nm}$	15-24	14-23	14-33	-	-
50 nm Vesicle					
$d_i/\text{nm}$	10 - 50	6 - 42	6 - 35	13 - 34	-
$d_o/\text{nm}$	16 - 97	15 - 86	17 - 41	19 - 40	-

tive of  $F_0$  with respect to the number of fluid lipids is therefore a constant at a given temperature; as  $T_m = 302$  K<sup>20</sup>, the bulk tendency opposes melting at all temperatures where incomplete melting was observed.

The interfacial contribution to the free energy also promotes melting here, because for the faceted geometry, melting decreases the area of each domain and thus the length of its boundary. We can assume that  $F_{interf}$  is given by the product of a line tension  $\Lambda$  and the length of the interface, which for a single circular domain scales as  $(N_{domain} a_g)^{1/2}$ . The change in  $F_{interf}$  with respect to melting in a single bilayer leaflet is:

$$\frac{dF_{interf}}{d\Delta N} = -\frac{\Lambda}{4} \left( \frac{\pi a_g}{N_{domain}} \right)^{1/2} \quad (11)$$

That is, the driving force towards melting due to the line tension increases as melting proceeds. It cannot therefore be responsible for the slowing-down of melting (unless the number of domains changes).

Equating the tendency of the line tension to shrink the gel-phase domain (Equation 11) with the bulk tendency to add lipids to it (Equation 10) yields a temperature-dependent critical size, below which the (monolayer) domain is unstable:<sup>41</sup>

$$N^* = \pi a_g \left( \frac{\Lambda/2}{\Delta H (1 - T/T_m)} \right)^2 \quad (12)$$

Using the most recently obtained values for the transition temperature,<sup>20</sup> enthalpy of melting,<sup>20</sup> and line tension,<sup>20,42</sup> the critical diameters of gel-phase domains at the temperatures of interest have been calculated and are given in Table 4. In cases where partial melting is seen, the final domain sizes begin and remain above the critical domain size calculated at that temperature. So, while line tension is undoubtedly an influence on the melting rates, it cannot account for the abrupt decrease in melting rate in the first 20 ns or the more graduate slowing down over 100's of ns seen in experiment and simulation.

Thermal expansion of the internal solvent is a possible source of initial rapid partial melting, but the degree of expansion over the temperature jumps is limited to 1.1 – 1.8% as the linear fit in the

solvent volume ( $\text{nm}^3/\text{bead}$ ) as a function of temperature shows:  $v_{sol} = 0.09234 + 0.000147T$ . Approximating the vesicle as spherical, the change in the surface area of the vesicle  $\Delta A_{melt}$  due to solvent expansion, the change in the surface area per lipid transitioning from the gel phase to the fluid phase  $\Delta a_{melt}$ , and the number of lipids  $N_{Lip}$  in the vesicle can be used to calculate the change in the fraction of lipids in the gel phase:

$$\begin{aligned} \Delta Gel &= \frac{-2(\Delta A_{melt}/\Delta a_{melt})}{N_{Lip}} \\ &= \frac{-2(36\pi)^{1/3} \left( (n_{sol}v_{sol,H})^{2/3} - (n_{sol}v_{sol,C})^{2/3} \right)}{N_{Lip} (a_f - a_g)}, \end{aligned} \quad (13)$$

where  $n_{sol}$  is the number of coarse grained solvent particles encapsulated by the vesicle,  $v_{sol,C}$  and  $v_{sol,H}$  are the volume per solvent bead for the temperatures before and after the T-jump, and the areas per lipid for the gel and fluid phase are respectively  $a_f$  and  $a_g$ . The solvent expansion as such would result in a decrease of 1.5–2.3% for the small vesicle and 1.7–2.9% by comparison to that seen in Fig. 8. Thus solvent expansion alone cannot account for the 20 ns of rapid initial melting.

The coupling of degree of melting to curvature is difficult to treat formally except under the idealized case of a straight ridge of constant curvature (i.e., a section of a cylinder) that joins two flat gel-phase domains that maintain a fixed relative angle  $\theta$ . The radius of curvature of a ridge of length  $L$  containing  $N_f$  lipids is  $N_f a_f (L\theta)^{-1}$ .

$$F_{curv} = \frac{\kappa N_f a_f}{2 r^2} = \kappa \frac{L^2 \theta^2}{2 N_f a_f} \quad (14)$$

At a fixed angle between facets and ridge length, increasing  $N_f$  lowers  $F_{curv}$ :

$$\frac{dF_{curv}}{dN_f} = -\frac{\kappa}{2a_f} \left( \frac{L\theta}{N_f} \right)^2 \quad (15)$$

As the number of fluid-phase lipids  $N_f$  increases, the favorable contribution of curvature stress towards bending becomes weaker. This is therefore the only free energy contribution that can account for the decrease in melting rate observed in the simulations after the initial  $\sim 20$  ns, over which the 2-d shapes of the domains and the 3-d shapes of the vesicles do not qualitatively change (see Figs. S4 and S5) and the mean domain size decreases (as indicated by the increase in ratio of interfacial to gel-phase lipids, Fig. 11 C). For the larger vesicle heated to 290 K, this accounts for nearly the entire extent of the observed melting. In all other cases where partial melting is seen the melting proceeds in concert with shape changes over the remainder of the 500 ns trajectories, as evident in the final structures in Figs. 9 and 10, and in comparing time dependences of the relative shape anisotropy (Fig. 11 A) and the degree of melting (Fig. 8).

In general, once the fluid zones separating gel-phase domains are wide enough, the domains can adopt more compact structures (less constrained by the edges of the overall polyhedral structure) and can migrate to form a different arrangement of domains and/or fuse with others. Furthermore, complete melting of an isolated domain was seen in some cases which is expected once

melting brings the domain size below the critical nucleus size.

In the case of the 300 K vesicle, the inner leaflet domain sizes are below the critical nucleus size which could in part account for the vesicle melting so rapidly that the shape change lags behind. Values for the 50 nm vesicle (Table 4) are also above the critical domain sizes.

For T-jumps to temperatures above (310 K) or slightly below (300 K) the planar bulk transition temperature, the initial domain sizes are either below the critical nucleus size or near enough that a small amount of shrinkage brings them below, producing complete melting. The shapes of the vesicles continue to evolve after melting is complete, in the case of the smaller vesicles reaching a peanut- or dumb-bell shaped, approximately prolate structure that persists for hundreds of nanoseconds. (The larger 300 K vesicle is continuing to evolve at the end of the trajectory, but the changes in its moments of inertia (Fig. S8) are consistent with an approach to a prolate structure.)

Seifert et al.<sup>38</sup> used two different models to construct phase diagrams for elastically stable structures for vesicles subjected to a full range of deflated volumes, the spontaneous-curvature model and the coupled bilayer model.

To make a comparison to the phase diagrams produced by Seifert et al.<sup>38</sup>, we calculated the corresponding reduced area difference,  $\Delta a$ , and reduced volume,  $v$ , variables based on our simulations. These two variables are normalized with respect to a spherical, fully hydrated vesicle with the same number of lipids. The radius  $R_0$  is related to the fully melted and hydrated vesicle such that,

$$R_0 = (A/4\pi)^{1/2} = \left( \frac{N_{inner} a_f}{4\pi} \right)^{1/2}, \quad (16)$$

where  $N_{inner}$  is the number of inner leaflet lipids and  $a_f$  is the area per lipid in the fluid phase. The reduced volume variable is:

$$v = \frac{V}{4\pi/3 R_0^3}, \quad (17)$$

where  $V$  is the vesicles actual encapsulated volume. The 33 nm vesicle encapsulates approximately 87,250 solvent particles. At a temperature of 300 K, the solvent density is 7.41 beads/ $\text{nm}^3$  and the vesicle volume is 11,648.6  $\text{nm}^3$ . The radius of the inner leaflet of a vesicle with the same lipid population in the fluid phase and full hydration is calculated to be 16.7 nm and the reduced volume for the fully melted vesicle at 300 K is 0.59.

The area difference between the leaflets  $\Delta A$ ,

$$\Delta A = A^{outer} - A^{inner} = (f^{outer} - f^{inner}) N_{Lip} * a_f, \quad (18)$$

where  $f^{outer}$  and  $f^{inner}$  are the fractions of lipids in the inner and outer leaflets respectively, is related to the integrated mean curvature  $M$  and distance between the leaflets  $D$  such that  $M \approx \Delta A/2D$ . Thus the reduced area is:

$$\Delta a = \frac{M}{4\pi R_0} \approx \frac{\Delta A}{8\pi D R_0} \quad (19)$$

The actual value of  $\Delta a$  is highly sensitive to the definition of  $D$ , which depends on the reference plane. The ‘‘pivotal plane’’ is defined such that the number of lipids in a curved leaflet is pro-

**Table 5** Relative volume  $v$  and change in area  $\Delta a$  parameters for comparison to the phase diagrams produced by Seifert et al.<sup>38</sup> as they apply to the fully vesicles at 300 K.

$N_{Lip}$	$R_0/nm$	$V/nm^3$	$v$	$\Delta a$
13,165	16.7	11648.6	0.59	1.48
31,021	26.6	48783.0	0.62	1.42

portional to its area.<sup>43</sup> It has been calculated for MARTINI DMPC as 0.85 nm away from the midplane, or 0.89 nm closer to the midplane than the mean distance of the phosphate beads.<sup>43</sup> For MARTINI DPPC, in which the phosphate beads lie at 2.0 nm from the midplane,<sup>14</sup> we may therefore estimate that the pivotal plane is at 1.11 nm from the midplane, and the effective thickness of the bilayer is 2.22 nm. The reduced area difference then is  $\Delta a = 1.48$  for the smaller vesicle and 1.42 for the larger. Fluid vesicles with these combinations of  $v$  and  $\Delta a$  are predicted to adopt a prolate dumb-bell shape according to the phase diagram calculated by Seifert et al.<sup>38</sup> The final structures of smaller vesicles simulated at 300 and 310 K (shown in Fig. 9) are consistent with this prediction. The larger vesicle at 300 K appears as a pear-shaped structure after 500 ns CG simulation (Fig. 10), but its shape is clearly still changing (as evident from its anisotropy parameter, shown in Fig. 11 A) and it is reasonable to assume it will adopt a similarly symmetric prolate shape as well. Using  $D = 4.0$  nm in Equation 19 yields  $\Delta a$  values near 0.8, which would be predicted to produce cup-like stomatocyte shapes.

For both vesicle sizes, the shape change lags behind the vesicle phase transition. We can surmise as a result that the driving force behind the melting is larger than the barrier incurred by a high curvature energy surface ‘transition state’. Ultimately, the fully melted vesicles would be expected to adopt spherical shapes over timescales long enough for solvent permeation and lipid flip-flop to remove the effective constraints on  $v$  and  $\Delta a$  respectively.

### 3.5 Topological Evolution

Changes in curvature occur in two ways - melting at pre-existing gel-fluid interfaces along the edges of the vesicle and changes in the number and arrangement of gel domains. In this section we will discuss some of the more interesting trends in the topological events of vesicles that undergo partial melting.

There are two mechanisms observed that facilitate a change in the number of domains: complete melting of a domain (inner and outer) and the fusion/fission of domains. In the first case, the inner leaflet domain is the first to melt completely. With a smaller domain size, a higher curvature and a different orientation of lipids with respect to that curvature, the melting phase transition is favored by the inner leaflet. The outer leaflet can persist for tens of nanoseconds but eventually melts.

Examples of domain fusion can be seen in Fig. S7 (see supplement, domain A). In the equilibration of the smaller 33 nm vesicle, a single outer leaflet domain merged together to bridged two inner leaflet domains. The evolution of the domain’s continued fusion in the first case at 290 K shows that one of the inner domains has to melt completely before the remaining one is permitted to grow and become a single mirroring domain. Alternately

in the case of the vesicle at 295 K, the two inner domains melt completely followed by the outer leaflet domain.

Domain fission is shown in Fig. S7 (see supplement, domain B) as the other direction that a bridging domain can take. The vesicle at 290 K first undergoes fission of the outer leaflet domain. The smaller inner leaflet domain melts completely and is then followed by its mirroring outer leaflet domain. For the vesicle at 295 K the same domain in the outer leaflet undergoes a similar process except the remaining outer leaflet domain then fuses with a different neighboring domain in the outer leaflet followed by complete melting of the smaller inner domain to form a single pair of inner and outer leaflet domains.

Based on these observations, the fusion of two domains is more easily accomplished through the outer leaflet. Subsequently one of the inner leaflet domains has to melt to facilitate a transition to a single set of inner and outer leaflet domains. Coupling between the leaflets and the curvature environment of the inner leaflet prevent them from migrating or growing until forming contact. Similar dynamics were seen in the larger vesicle as shown in Fig. S7 (see supplement, domains C and D).

### 3.6 Refreezing

In the experiments performed by Nagarajan et al. a temperature jump (T-jump) is affected over a 10 ns dead time during which there are no IR measurements. The dynamics of the melting is then probed using time resolved infrared spectroscopy (TRIR) over  $10^9$  to  $10^2$  s.<sup>5</sup> It is assumed that the sample remains at a constant temperature for approximately 12 ms before it cools via diffusion of heat.<sup>6</sup>

Thus if the experiments involve cycles of heating and cooling, does the vesicle reach a true equilibrium structure or simply vacillate between two meta-stable states? By extension, this brings into question whether the initial structure of the vesicles with many domains used here, accurately represents the structure of a vesicle in the cool part of the heating cycle.

To address the question of reversibility in light of the changes in shape and number of domains, we refreeze the small SUV structure at 295 K to 280 K. The vesicle structure at 295 K is considered the most interesting case with an almost oblate symmetry and the most extreme shape change of the partially melted SUVs (see Fig. 11 A). The outer leaflet has 3 gel domains while the inner leaflet has 2 gel domains, thus presenting a situation where one of the gel domains does not have a mirror in the inner leaflet.

Images of the initial and final structures of the vesicle are displayed in Fig. 12 from four viewpoints looking down the  $I_A$ ,  $I_B$ , and  $I_C$  moment of inertia principle axes of the 280 K vesicle after 1  $\mu$ s of simulation.

The total number of domains in the inner and outer leaflets does not change in the 1  $\mu$ s simulation. The domains all grow in size with the total percentage of lipids in the gel phase almost recovering completely at 54.3% (Table 2). The refreezing process is slower than the melting process as seen in Fig. 13 A. We propose that the rate of freezing after the initial increase in the fraction of gel phase lipids is tempered by processes governing changes in the vesicle curvature such as domain nucleation and fission.

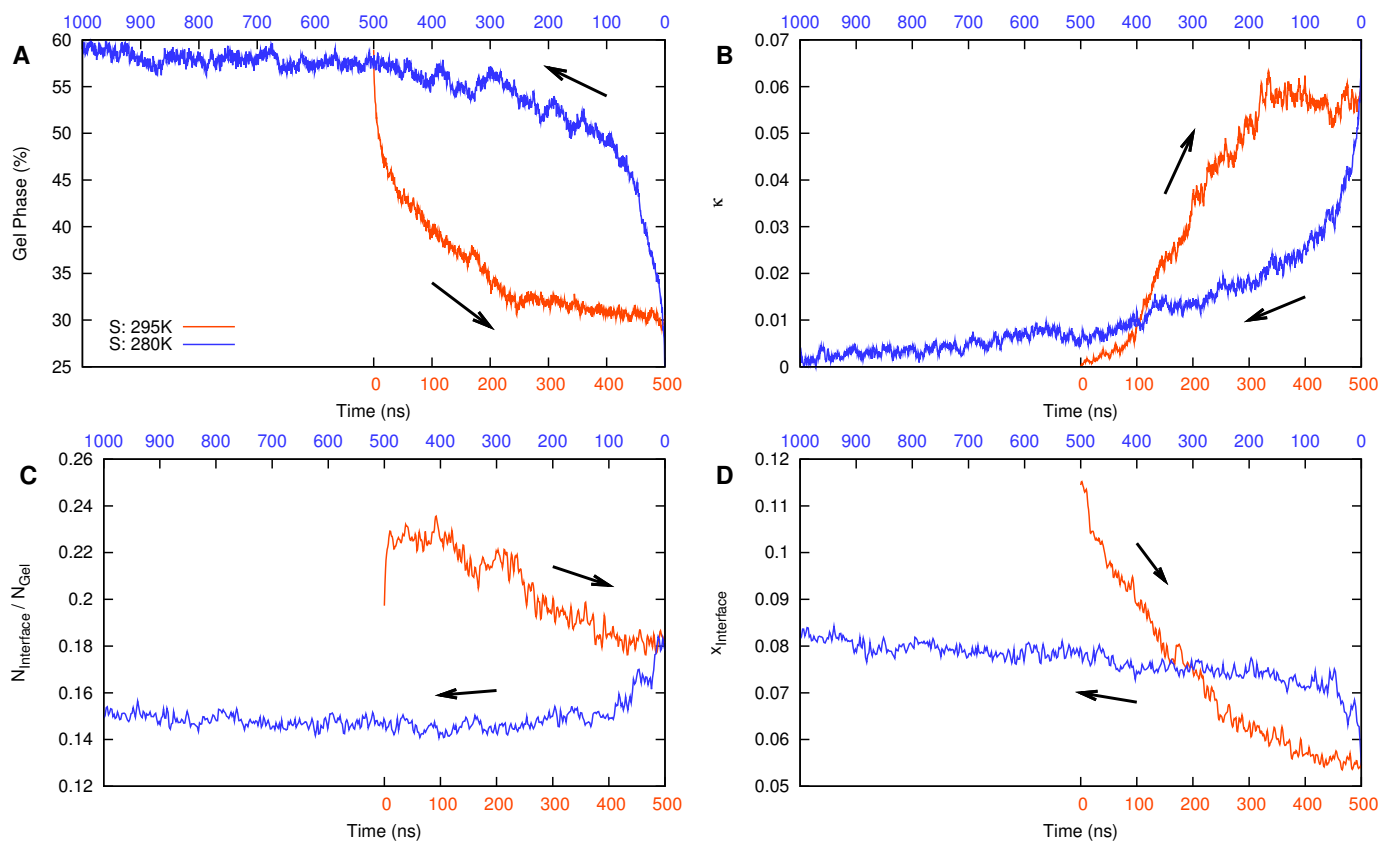


**Fig. 13** Plots of the percentage of lipids in the gel phase (A) and the relative shape anisotropy (B), the fraction of gel phase lipids at a gel-fluid interface (C) and the absolute fraction of lipids at a gel-fluid interface (D) for the vesicle melting at 295 K (orange) and subsequent refreezing at 280 K (blue).

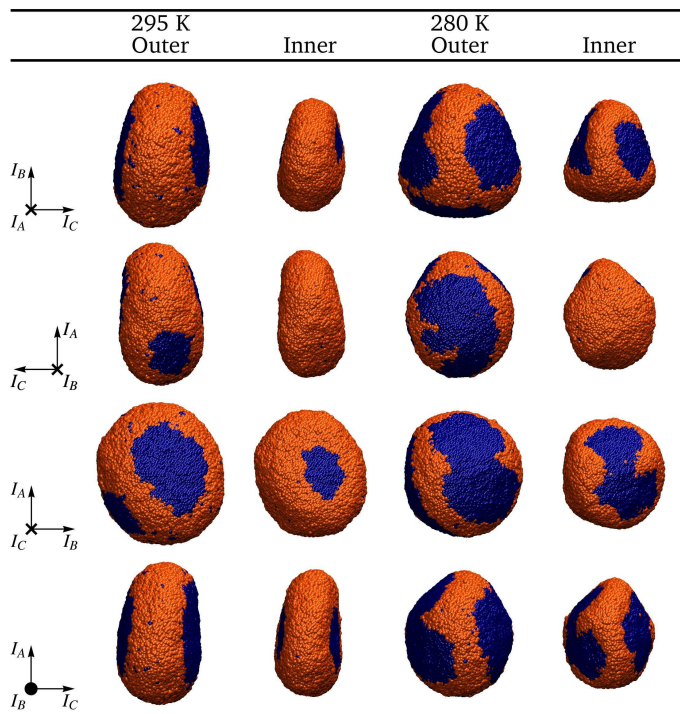


**Fig. 12** Snapshots of the 33 nm vesicle's inner and outer leaflets at 295 K (left) and at the end of a 1  $\mu$ s refreezing simulation at 280 K (right).

The domain shown in the third row in Fig. 12 and on the left hand side of the fourth row images is mirrored across the inner and outer leaflets. The process of splitting the domain is facilitated in part by the domains bending outwards so that the lipids melt along the 'hinge' - a forming edge between two facets. This would suggest that given more time, the vesicle will revert to a structure with more domains. In Fig. 13 B the relative shape anisotropy demonstrates a reversion to a relatively spherical symmetry that is facilitated by the bending, splitting, and growth of domains.

The outer leaflet gel domain shown in the second row of Fig. 12 lacks a mirroring gel domain in the inner leaflet from start to finish, although the outer domain grows quite large upon refreezing. This would confirm that the nucleation of a gel domain in the inner leaflet is a rare event. The nucleation event is hampered by the curvature of the inner leaflet. The same domain can be seen from the side on the left side of the vesicle in the third row. The size of the outer leaflet domain and rigidity of the gel phase promotes flattening of a portion of the inner leaflet. Although not seen in simulation, given enough time the flattened portion could facilitate a gel domain nucleating on the inner leaflet, thus stabilizing the gel domain in the outer leaflet.

Fig. 13 C shows that the fraction of gel lipids at the interface initially decreases as a result of the growth of a fixed number of gel domains. The absolute fraction of interfacial lipids (Fig. 13 D) has a fast initial growth followed by a steady increase, indicating that the refreezing process does not reach a steady state within the simulation time.

### 3.7 Implications for dynamics beyond 500 ns

Although our simulations capture only the initial stages of melting following an ultrafast temperature jump, based on our observations we may speculate about the later stages. We hypothesize that the system approaches a plateau level of melting where the bending, interfacial, and intrinsic effects of further melting balance out, and that this accounts for the initial single-exponential phase of melting observed experimentally. Fluctuations around this degree of melting (or fluctuations in the partitioning of the gel phase fraction among multiple domains) will continue. The permeation of solvent on a time scale of  $10^{-2}$  s is likely too slow to account for the subsequent stretched exponential. Infrequent large fluctuations may break the stability of the arrangement of domains, provoking (for instance) the complete melting of a domain and the rearrangement of the remaining gel domains, which will adopt a new plateau level of melting. Such rare events with high activation barriers could account for the stretched-exponential melting component observed in experiment. While the permeation of solvent (and associated volume expansion) is expected to have a profound effect on the shape and phase composition of the fully equilibrated vesicle structure, with a time scale of  $10^{-2}$  s it is apparently too slow to account for the melting in this regime, approximately half of which takes place between  $10^{-6}$  and  $10^{-5}$  s.<sup>5</sup>

## 4 Conclusions

Vesicles with diameters of 33 nm and 50 nm are equilibrated to form faceted frozen topologies in agreement with previous simulations. The inner leaflet displays a greater degree of conformational disorder than the outer leaflet.

Vesicles that undergo partial melting at temperatures below 300 K exhibit single exponential kinetics in qualitative agreement with experiment, accompanied by shape changes driven by changes in the surface area to volume ratio and curvature stress. The internal volume of the vesicle is constant over the time scale of the phase transition due to the low permeability of the bilayer to solvent, as lipids convert from the gel phase to the fluid phase, the surface area of the vesicle increases. This initial conversion serves to decrease the local curvature of the edges on the faceted structure where the fluid phase is localized. Further melting after the first ( $\sim 20$ ns) relaxation changes curvature stress until a domain is fully melted or merges with a neighboring domain, changing the vesicle shape and thus the curvature stress free energy surface, thereby influencing the melting rates of other domains.

Further significant melting will then occur upon rare fluctuations large enough to change the number of domains (complete melting or fusion). The large and heterogeneous barriers to such events may contribute to the stretched exponential nature of the slow phase of melting observed in experiment.

Vesicles that undergo full melting have distinctly different kinetics since the driving force behind the phase transition exceeds the barrier created by a build up of stresses. The final structures of these vesicles assume the prolate symmetry of a dumbbell shaped surface, a shape that has been found as a minimum curvature energy surface in previous studies using the bilayer-coupling model.<sup>38</sup>

Finally the refreezing of a partially melted vesicle would indicate that the cycles of heating and cooling of vesicles using T-jumps and TRIR would not simply cause existing domains to grow and shrink but for there to be significant topological changes in the number of domains present on the surface of the vesicle. This supports the hypothesis that the phase transition temperature and thus the rate of melting in the single exponential phase of the melting kinetics is a dependent on the curvature energy of the vesicle.

## 5 Acknowledgements

This research was supported by the National Science Foundation (NSF) under grant No. CHE-1213904 and the American Chemical Society Petroleum Research Fund (ACS-PRF) grant No. 54642-ND6. Simulations were performed using the Extreme Science and Engineering Discovery Environment (XSEDE) computing resources Trestles and Comet, which is supported by NSF grant No. ACI-1053575, and the resources of the Cherry L. Emerson Center for Scientific Computation.

## References

- 1 C. M. Lin, C. S. Li, Y. J. Sheng, D. T. Wu and H. K. Tsao, *Langmuir*, 2012, **28**, 689–700.
- 2 M. Hossann, Z. Syunyaeva, R. Schmidt, A. Zengerle, H. Eibl, R. D. Issels and L. H. Lindner, *Journal of Controlled Release*, 2012, **162**, 400–406.
- 3 J. P. May and S. D. Li, *Expert Opinion on Drug Delivery*, 2013, **10**, 511–527.
- 4 D. W. Deamer and J. Bramhall, *Chemistry and Physics of Lipids*, 1986, **40**, 167–188.
- 5 S. Nagarajan, E. E. Schuler, K. Ma, J. T. Kindt and R. B. Dyer, *Journal of Physical Chemistry B*, 2012, **116**, 13749–13756.
- 6 R. B. Dyer, F. Gai, W. H. Woodruff, R. Gilmanshin and R. H. Callender, *Accounts of Chemical Research*, 1998, **31**, 709–716.
- 7 M. Andersson, L. Hammarstrom and K. Edwards, *Journal of Physical Chemistry*, 1995, **99**, 14531–14538.
- 8 H. J. Risselada and S. J. Marrink, *Soft Matter*, 2009, **5**, 4531–4541.
- 9 E. J. Spangler, P. B. S. Kumar and M. Laradji, *Soft Matter*, 2012, **8**, 10896–10904.
- 10 L. S. Hirst, A. Ossowski, M. Fraser, J. Geng, J. V. Selinger and R. L. Selinger, *Proc Natl Acad Sci U S A*, 2013, **110**, 3242–3247.
- 11 H. L. Wu, Y. J. Sheng and H. K. Tsao, *J Chem Phys*, 2014, **141**, 124906.
- 12 R. Sknepnek, G. Vernizzi and M. O. de la Cruz, *Soft Matter*, 2012, **8**, 636–644.
- 13 M. J. Bowick and R. Sknepnek, *Soft Matter*, 2013, **9**, 8088–8095.
- 14 S. J. Marrink, A. H. de Vries and A. E. Mark, *The Journal of Physical Chemistry B*, 2004, **108**, 750–760.
- 15 S. J. Marrink, H. J. Risselada, S. Yefimov, D. P. Tieleman and A. H. de Vries, *J Phys Chem B*, 2007, **111**, 7812–24.
- 16 J. F. Nagle and D. A. Wilkinson, *Biophysical Journal*, 1978, **23**, 159–175.
- 17 R. Lewis, W. Pohle and R. N. McElhaney, *Biophysical Journal*, 1996, **70**, 2736–2746.
- 18 M. V. Fraile, B. Patron-Gallardo, G. Lopez-Rodriguez and P. Carmona, *Chemistry and Physics of Lipids*, 1999, **97**, 119–128.
- 19 H. Singh, J. Emberley and M. R. Morrow, *European Biophysics Journal with Biophysics Letters*, 2008, **37**, 783–792.
- 20 L. Yang and J. T. Kindt, *Submitted to Phys. Chem. Chem. Phys.*, 2015.
- 21 J. F. Nagle, R. T. Zhang, S. Tristram-Nagle, W. J. Sun, H. I. Petrache and R. M. Suter, *Biophysical Journal*, 1996, **70**, 1419–1431.
- 22 H. I. Petrache, S. W. Dodd and M. F. Brown, *Biophys J*, 2000, **79**, 3172–92.
- 23 J. F. Nagle, *Biophys J*, 1993, **64**, 1476–1481.
- 24 W. Sun, R. M. Suter, M. A. Knewtonson, C. R. Worthington, S. Tristram-Nagle, R. Zhang and J. F. Nagle, *Physical Review E*, 1994, **49**, 4665–4676.
- 25 W. J. Sun, S. Tristram-Nagle, R. M. Suter and J. F. Nagle, *Biophysical Journal*, 1996, **71**, 885–891.
- 26 R. P. Rand and V. A. Parsegian, *Biochimica Et Biophysica Acta*, 1989, **988**, 351–376.
- 27 J. C. Mathai, S. Tristram-Nagle, J. F. Nagle and M. L. Zeidel, *Journal of General Physiology*, 2008, **131**, 69–76.
- 28 H. J. C. Berendsen, D. van der Spoel and R. van Drunen, *Computer Physics Communications*, 1995, **91**, 43–56.
- 29 D. Van Der Spoel, E. Lindahl, B. Hess, G. Groenhof, A. E. Mark and H. J. C. Berendsen, *Journal of Computational Chemistry*, 2005, **26**, 1701–1718.
- 30 B. Hess, C. Kutzner, D. van der Spoel and E. Lindahl, *Journal of Chemical Theory and Computation*, 2008, **4**, 435–447.
- 31 S. Pronk, S. Páll, R. Schulz, P. Larsson, P. Bjelkmar, R. Apostolov, M. R. Shirts, J. C. Smith, P. M. Kasson, D. van der Spoel, B. Hess and E. Lindahl, *Bioinformatics*, 2013, **29**, 845–854.
- 32 G. Bussi, D. Donadio and M. Parrinello, *Journal of Chemical Physics*, 2007, **126**, 014101.
- 33 H. J. C. Berendsen, J. P. M. Postma, W. F. van Gunsteren, A. DiNola and J. R. Haak, *Journal of Chemical Physics*, 1984, **81**, 3684–3690.
- 34 W. Humphrey, A. Dalke and K. Schulten, *J. Mol. Graphics*, 1996, **14**, 33–38.
- 35 D. N. Theodorou and U. W. Suter, *The Journal of Chemical Physics*, 1985, **82**, 955.
- 36 J. Vymetal and J. Vondrasek, *Journal of Physical Chemistry A*, 2011, **115**, 11455–11465.
- 37 A. Lamberg and T. Taniguchi, *Soft Matter*, 2014, **10**, 257–261.
- 38 U. Seifert, K. Berndl and R. Lipowsky, *Physical Review A*, 1991, **44**, 1182–1202.
- 39 V. D. Gordon, P. A. Beales, Z. Zhao, C. Blake, F. C. MacKintosh, P. D. Olmsted, M. E. Cates, S. U. Egelhaaf and W. C. K. Poon, *Journal of Physics: Condensed Matter*, 2006, **18**, L415.
- 40 S. Schneider and G. Gompper, *Europhysics Letters*, 2005, **70**, 136.

- 41 S. J. Marrink, J. Risselada and A. E. Mark, *Chemistry and Physics of Lipids*, 2005, **135**, 223–244.
- 42 S. Katira, K. K. Mandadapu, S. Vaikuntanathan, B. Smit and D. Chandler, *arXiv preprint arXiv:1506.04298*, 2015.
- 43 X. Wang and M. Deserno, *J Chem Phys*, 2015, **143**, 164109.

# Graphical Abstract

## Coarse-grained molecular simulations of the melting kinetics of small unilamellar vesicles

Lara A. Patel, and James T. Kindt

Frozen lipid vesicles simulated using a coarse-grained potential and subject to temperature jumps respond by melting on timescales similar to those observed experimentally; changes in curvature stress appear to play a dominant role in controlling the melting rate.

